Computed Tomographic Study on Internal Structure of a Diesel Spray Impinging on a Flat Wall

H.Hiroyasu, K.Nishida and J.C.Min
Department of Mechanical Engineering
University of Hiroshima
Shitami, Saijo-cho
Higashi-Hiroshima 724
Japan
M.Arai
Gunma University
H.Yoshida
Maritime Safety Academy

ABSTRACT

A focused shadow photographic analysis was combined with a computed tomographic transformation for the measurement of the fuel distribution inside diesel sprays impinging non-vertically on a flat wall. Areas with a high equivalence ratio existed at the impingement point and just behind the tip of the spray penetrating along the wall. The areas with a high equivalence ratio in the section parallel to the wall were distributed zonally along the spray tip and was shaped like a crescent. The maximum equivalence ratio at the spray tip on the wall was higher on the side of the wall which was at a larger angle to the nozzle hole axis than on the opposite side. Such a tendency became evident as the impingement angle increased. When the impingement angle exceeded a certain degree, the spray hardly penetrated in the direction at a smaller angle to the nozzle hole axis.

INTRODUCTION

An understanding of the mixture formation and combustion in small, direct injection (D.I.) diesel engines requires detailed information on the spatial fuel distribution and the physical structure of the spray injected into the combustion chamber, especially the spray impinging on the piston cavity wall, since much of the mixture formation is performed in the impinging spray. The dispersion and tip penetration of the vertically-impinging sprays along the wall were measured by direct photography(1). Attempts to analyze the fuel distribution in the vertically-impinging sprays were made by the image processing technique of a focused shadow photograph(2). Most of the sprays in the actual combustion chamber, however, impinge non-vertically on the piston cavity wall due to restrictions in the arrangement of the nozzle. The dispersion and tip penetration of such non-vertically impinging sprays were measured(3), whereas the fuel distribution in the sprays along the wall was not yet investigated.

Recently, there have been some attempts to determine the fuel distribution in the non-axisymmetric spray without the wall impingement by using a focused shadow photographic analysis, combined with a computed tomographic transformation (4)-(6). In this paper, an application of this technique to the sprays non-vertically impinging on a flat wall was made so as to clarify the effects of the wall impingement on the mixture formation process.

EXPERIMENTAL APPARATUS AND PROCEDURE

Pressure Bomb and Optical Arrangement

Figure 1 shows the pressure bomb and the optical arrangement of the focused shadow photography. The interior of the pressure bomb had a cylindrical shape of 100 mm diameter and 1400 mm length. Two Pyrex glass windows were installed in both sides of the bomb for optical access. A nozzle for the D.I. diesel engine and a flat wall were installed in the middle of the bomb. The nozzle had a single hole which was drilled at an angle with respect to the nozzle axis. The fuel used was diesel fuel. The ambient gas was ordinary air at room temperature and had a pressure of 1.3 MPa which simulated the ambient air density in the combustion chambers of D.I. diesel engines at the fuel injection timing.

To be able to observe the spray from many directions around the nozzle, the nozzle was installed on a turntable attached to the pressure bomb so that the injection direction might be capable of rotary movement around the nozzle axis. The injection pipes from the nozzle and from the injection pump were coupled by a rotary joint in order to avoid moving the imjection pump with the nozzle rotation.

The focused shadow images of the spray and the photographic step tablet were recorded

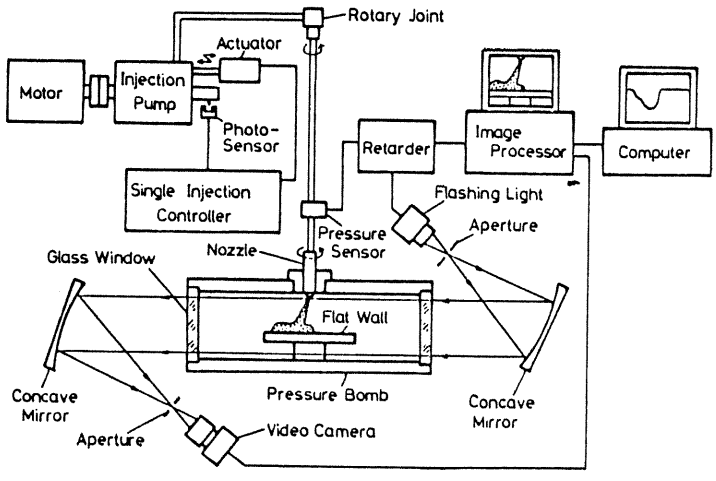

Fig.1 Experimental apparatus

simultaneously using a video camera. Quantization of the recorded gray image was made with the image processor, and the digitized image data was transferred to the computer. The image data acquisition was made from other directions around the nozzle. In this study, the nozzle was rotated in 3 degree increments around the nozzle axis, and sixty sets of projection data were obtained. Each data set was composed of seventy five point data at a 0.85 mm distance. The projection data was the average of three measurements.

Computed Tomographic Transformation

The data deconvolution process by the computed tomographic transformation is shown in Fig.2. The measurement of the transmissivity through the object (the line of sight focused shadow photographic density) $D_{shd}=\log(I_0/I)$ along the X-axis furnished one-dimensional projection data. The projection data matrix $g(X, \theta)$ was obtained by acquiring the projection data set from many directions around the object. By applying a filter function $h(x)$ for correction of the projection data, the filtered projection data matrix was calculated. Finally, the back projection of the filtered projection data matrix reconstructed the object image $f(x,y)$, that is, the photographic density $D(x,y)$. The convolution method using the filter function of Ramachandran et al.(7) was adapted as the algorithm for the reconstruction of the object image.

Quantitative Analysis of Fuel Concentration

The measuring technique for the fuel concentration in the spray was based on the incident light extinction principle(8). The local photographic density in the tomogram $D(x,y)$ was related to the local number density of drops $N(x,y)$ and the Sauter mean diameter d_{32} as in Eq.(1):

$$N(x,y) = \frac{2.303\ D(x,y)}{\frac{\pi}{4}\ d_{32}^{\ 2}\ Q_{ext}\ \Delta L} \qquad (1)$$

where ΔL : unit length of optical path
Q_{ext} : extinction coefficient.

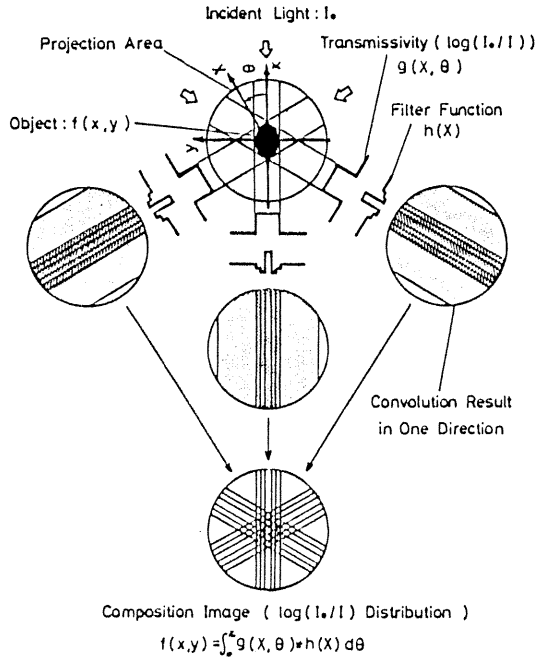

Fig.2 Data deconvolution process by a computed tomographic transformation

Q_{ext} was fixed at 2.0 in this study. The Sauter mean diameter was obtained by using a summation of the focused shadow photographic density in the entire spray ($\Sigma D_{shd} \Delta S$) and the mass of fuel in the spray M_f as follows :

$$d_{32} = \frac{0.63\ Q_{ext}\ M_f}{\rho_f\ (\Sigma\ D_{shd}\ \Delta S)} \qquad (2)$$

where ΔS : unit area
ρ_f : fuel density.

The local fuel concentration was obtained from the Sauter mean diameter and the local number density of drops. The mass of fuel in the spray M_f in Eq.(2) was obtained by subtracting the fuel adhering to the wall from the fuel injected by the sampling time.

RESULTS AND DISCUSSION

Figure 3 shows a schematic of the spray impinging on the flat wall and symbols used in the description of the results. The impingement point was defined by the intersection of the nozzle hole axis and the wall. The impingement angle θ was defined by the angle between the nozzle hole axis, and a line normal to the wall at the impingement point. The impingement distance L was defined by the distance between the nozzle tip and the wall. The location of the tomogram of the spray by the computed tomographic analysis was expressed by Z, that is, the distance from the wall.

Table 1 shows the experimental conditions. Two kinds of nozzles were used in this study. One had a single hole with a hole diameter d_0=0.35 mm and an impingement angle θ=30 deg. (No.1, 2, 3), and the other had a single hole with a hole diameter d_0=0.25 mm and an impingement angle θ=15 deg. (No.4, 5). The nozzle opening pressure was fixed at 19 MPa. The impingement distance L was set at 13.4 mm and 20.0 mm. Analyses of the spray vertically impinging on the wall (No.2, with the

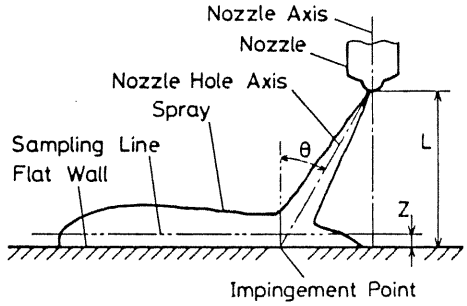

θ : Impingement Angle
L : Distance between Flat Wall and Nozzle
Z : Distance between Sampling Line and Flat Wall

Fig.3 Schematic drawing of an impinging spray

Table 1 Experimental conditions

No	Nozzle Hole Diameter d_0 (mm)	Impingement Angle θ (deg.)	Distance between Flat Wall and Nozzle L (mm)	Sampling time t (ms)	Ratio of Stuck Fuel (%)	Sauter Mean Diameter d_{32} (μm)
1	0.35	30	13.4	0.7	25.5	50.5
2	0.35	0	13.4	0.7	39.8	54.8
3	0.35	—	—	0.7	—	36.2
4	0.25	15	13.4	1.1	45.3	55.8
5	0.25	15	20.0	1.1	44.5	48.3

wall inclined) and the free spray (No.3, without the wall) were made for comparison. Since the image data acquisition from many directions by rotating the nozzle could not be made in these analyses (No.2, 3), the image data from one direction was used as the image data from other directions for the computed tomographic transformation.

Characteristics of Non-Vertically Impinging Spray

Figure 4 shows a focused shadow photograph of the spray at a time t=0.7 ms after the start of the injection. This was injected from the nozzle with a hole diameter d_0=0.35 mm and was impinged on the wall under the condition of an impingement angle θ=30 deg. and an impingement distance L=13.4 mm (No.1 Table 1). The photograph was taken from a direction normal to the plane which contains the nozzle axis. Analytical results of this spray are shown in Figs.5, 6 and 7. Figure 5 shows tomograms of the spray in the sections parallel to the wall at distances of Z=0.5 mm, 2.2 mm and 5.5 mm from the wall. The tomogram was represented by a contour map of equivalence ratios, consisting of four areas where the equivalence ratio was lower than 1.0, 1.0 to 2.5, 2.5 to 4.0, and higher than 4.0. The X-axis and the Y-axis were the center lines of the projection area, and the intersection of the X-axis and left-hand short line parallel to the Y-axis represented the location of the impingement point of the nozzle hole axis on the section. A tomogram of the spray in the section normal to the wall which contains the nozzle axis and the nozzle hole axis, is shown in Fig.6. The following characteristics of the non-vertically impinging spray could be drawn from these tomograms. The areas with a high equivalence ratio existed at the impingement point and just behind the tip of the spray penetrating along the wall. The areas with a high equivalence ratio in the section parallel to the wall were distributed zonally along the spray tip and were shaped like a crescent. It could be seen from Fig.6 that the areas with a low equivalence ratio were relatively wide in the part of the spray on the wall as compared with the part of the spray along the nozzle hole axis. The point with the highest equivalence ratio just behind the spray tip on the wall moved in the direction of the impingement point as the distance from the wall increased. Such a distribution of equivalence ratios implied that the vortex motion was induced by the interaction of the spray flow and the ambient gas.

Figure 7 shows a distribution of the equivalence ratios along the X-axis in the section shown in Fig.5. In the sections of Z=0.5 mm and 2.2 mm, the equivalence ratio had maximums at the nozzle hole axis, and just behind the spray tip on the wall on the left-hand side of the X-axis, whereas it did not have a maximum on the right-hand side of the X-axis. The equivalence ratio at the nozzle hole axis decreased as the section approached the wall from Z=5.5 mm to 0.5 mm.

Vertically-Impinging Spray and Free Spray

A vertically-impinging spray and a free spray were analyzed for comparison (No.2, 3 in Table 1). Figure 8 shows the focused shadow photographs of the vertically-impinging spray and the free spray. Figure 9 shows the tomograms of these sprays in the section which contains the nozzle axis and the nozzle hole axis. The thickness of the impinging spray on the wall showed the minimum at a certain

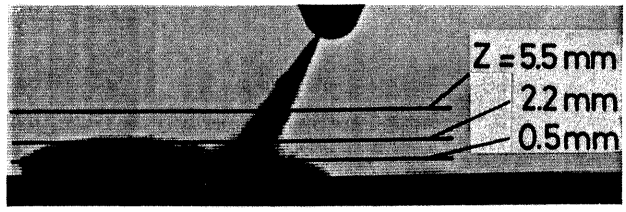

Fig.4 Shadow photograph of an impinging spray
θ=30 deg., L=13.4 mm, d_0=0.35 mm, t=0.7 ms

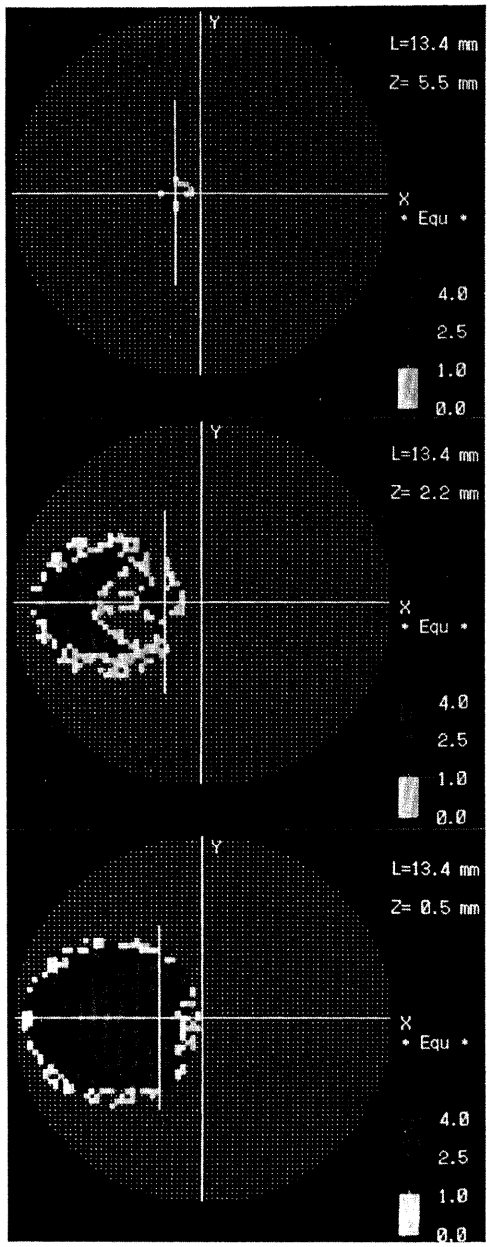

(1) Z=5.5 mm

(2) Z=2.2 mm

(3) Z=0.5 mm

Fig.5 Reconstructed tomograms of an impinging spray
(Contour maps of equivalence ratio
in sections parallel to the wall)

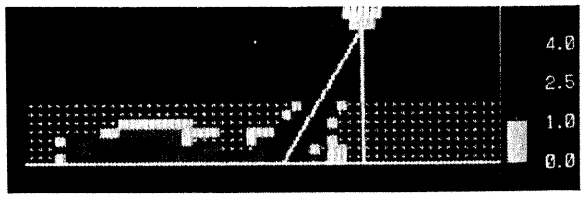

Fig.6 Reconstructed tomogram of an impinging spray
(Contour map of equivalence ratio
in a section normal to the wall)

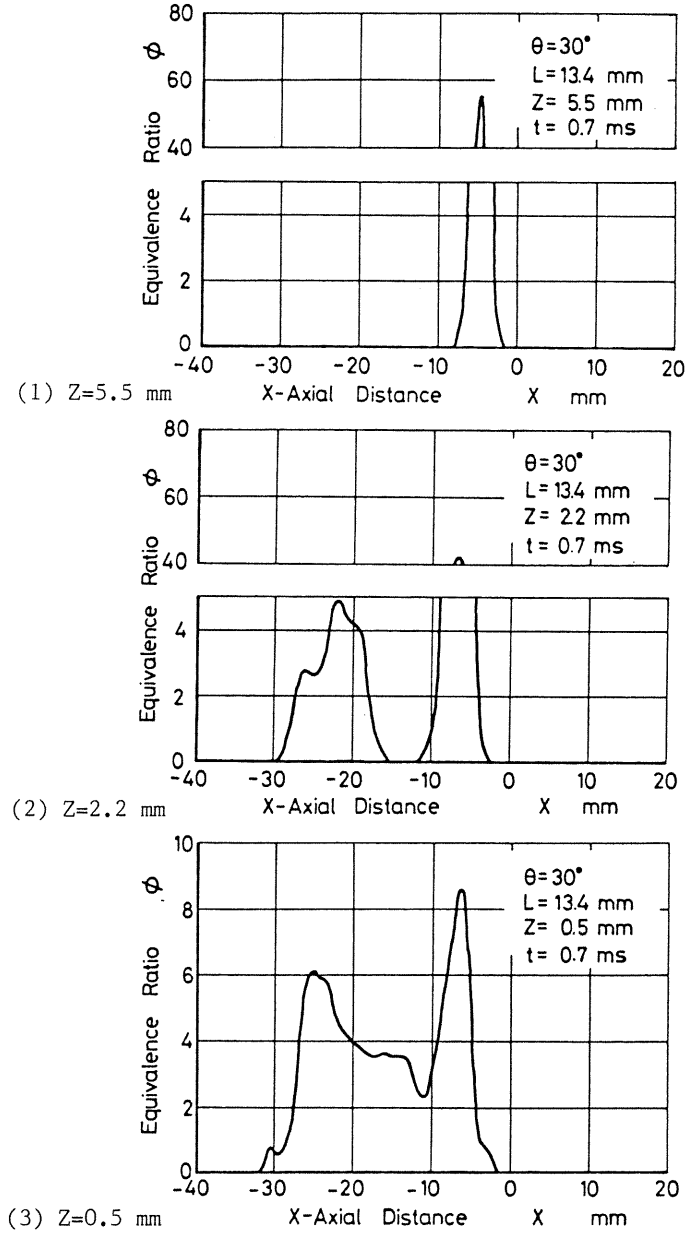

Fig.7 Distribution of equivalence ratio along X-axis in each section shown in Fig.5

distance from the impingement point. The distribution of a high equivalence ratio just behind the spray tip on the wall implied a vortex motion. Such characteristics of the vertically-impinging spray were quite similar to the non-vertically impinging spray shown in Fig.6.

The distributions of equivalence ratios along the X-axis in the section parallel to the wall are shown in Fig.10 for the vertically-impinging spray and the free spray. The equivalence ratio in the sections of Z=0.5 mm and 2.2 mm for the vertically-impinging spray had maximums at the impingement point and just behind the spray tip on the wall. The equivalence ratio at the nozzle hole axis decreased, as the section approached the wall from Z=5.5 mm to 0.5 mm. Such variations of the equivalence ratio were similar to the non-vertically impinging spray, too. The distributions of the equivalence ratio for both the vertically-impinging spray and the free spray did not differ so much in the sections of Z=2.2 mm and 5.5 mm, which were more distant from the wall than the thickness of the spray on the wall.

Effect of Impingement Angle and Impingement Distance on Spray Characteristics

Figure 11 shows a focused shadow photograph of the spray impinging on the wall under the condition of an impingement angle θ=15 deg. and an impingement distance L=13.4 mm (No.4 in Table 1). The sampling time was t=1.1 ms after the start of the injection. Figures 12 (1) and (2) show tomograms of the spray in the section parallel to the wall at a distance of Z=2.2 mm from the wall, and the tomogram of the spray in the section normal to the wall which contains the nozzle axis and the nozzle hole axis, respectively. As compared with the tomogram of the impinging spray under the condition of an impingement angle θ=30 deg. shown in Figs.5 and 6, much fuel spray penetrated in the direction which was at a smaller angle to the nozzle hole axis (in the right-hand direction) as well as in the opposite direction (in the left-hand direction). Figure 13 shows the distribution of the equivalence ratios along the X-axis in the section of Z=2.2 mm parallel to the wall. The maximum equivalence ratio at the spray tip on the wall was higher on the side of the negative X-axis, which was at a larger angle to the nozzle hole axis, than on the side of the positive X-axis, which was at a smaller angle to the nozzle hole axis.

A focused shadow photograph of the spray impinging on the wall under the condition of an impingement angle θ=15 deg. and an impingement distance L=20.0 mm (No.5 in Table 1) is shown in Fig.14. The analytical results are shown in Figs.15 and 16. As compared with the results under the condition of an impingement distance L=13.4 mm (Figs.12 and 13), both the impingement distances showed similar shapes of the tomogram of the spray in the section of Z=2.2 mm parallel to the wall. The impingement distance L=13.4 mm, however, showed a wider area with a low equivalence ratio in the tomogram than an impingement distance L=20.0 mm. A tomogram of the spray in the section normal to the wall which contained the nozzle axis and the nozzle hole axis revealed that, for the impingement distance L=20.0 mm, hardly any decrease in the thickness of the spray on the wall around the impingement point was evident, as compared with the impingement distance L=13.4 mm. The maximum equivalence ratio at the spray tip on the wall was a little lower for an impingement distance L=20.0 mm than for L=13.4 mm.

Sauter Mean Diameter

The Sauter mean diameters for the non-vertically and vertically-impinging sprays and the free spray are shown in the right-hand column of Table 1. The impinging spray showed a larger Sauter mean diameter than the free spray (No.1, 2, 3). The vertically-impinging spray showed a larger Sauter mean diameter than the non-vertically impinging spray (No.1, 2). The Sauter mean diameter increased as the impingement distance for the non-vertically impinging spray decreased (No.4, 5).

CONCLUSIONS

A focused shadow photographic analysis was combined with a computed tomographic transformation for the measurement of the fuel distribution inside diesel sprays impinging non-vertically on a flat wall. Tomograms of the sprays revealed several features of the impinging spray. The main results are as follows :

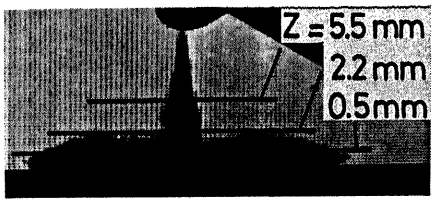

(1) Vertically-impinging spray
θ=0 deg., L=13.4mm, d_0=0.35 mm, t=0.7 ms

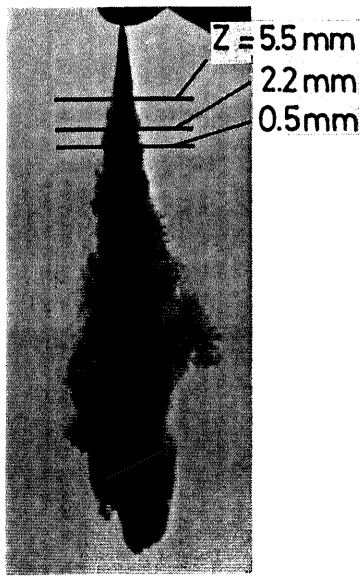

(2) Free spray
d_0=0.35 mm, t=0.7 ms

Fig.8 Shadow photographs of sprays

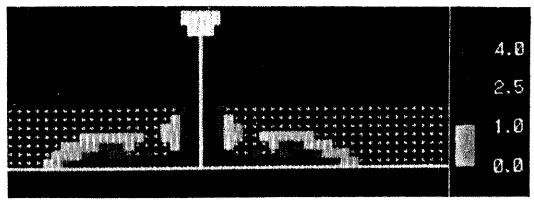

(1)Vertically impinging spray

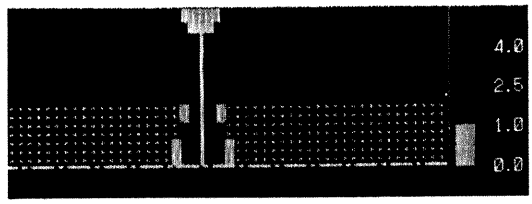

(2) Free spray

Fig.9 Reconstructed tomograms of sprays shown in Fig.8
(Contour maps of equivalence ratio in a section normal to the wall)

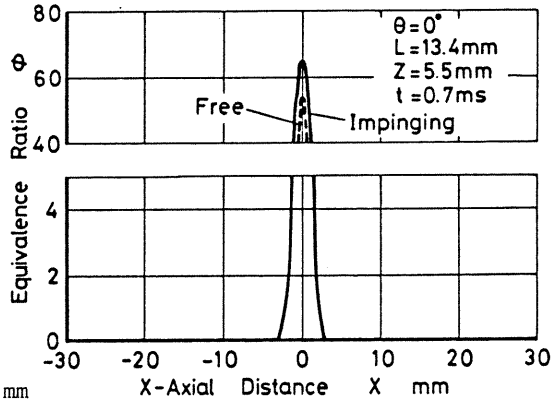

(1) Z=5.5 mm

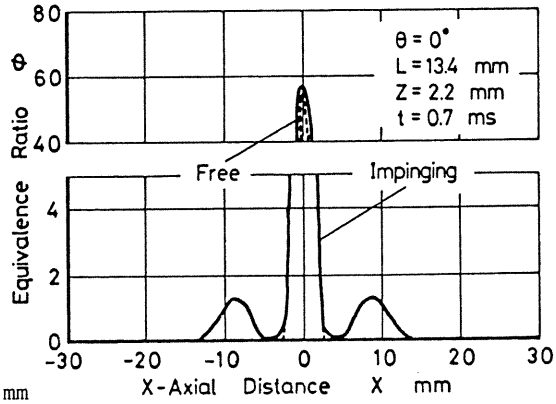

(2) Z=2.2 mm

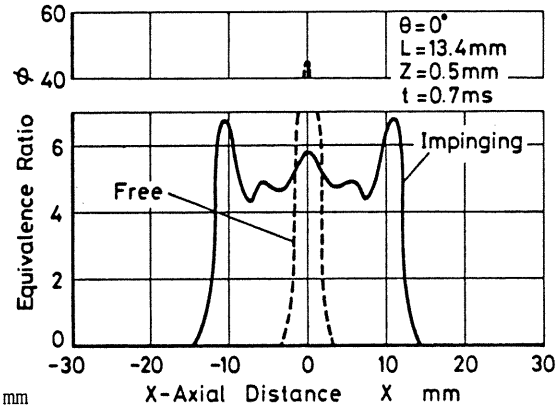

(3) Z=0.5 mm

Fig.10 Distribution of equivalence ratio along X-axis

(1) Areas with a high equivalence ratio existed at the impingement point and just behind the spray tip on the wall.
(2) Areas with a high equivalence ratio in the section parallel to the wall were distributed zonally along the spray tip and were shaped like a crescent.
(3) The maximum equivalence ratio at the spray tip on the wall was higher on the side of the wall which was at a larger angle to the nozzle hole axis than on the opposite side.
(4) When the impingement angle exceeded a certain degree, the spray hardly penetrated in the direction which was at a smaller angle to the nozzle hole axis.

ACKNOWLEDGMENT

The authors wish to thank Mr. Kenji Date for his effort during the experiment.

REFERENCES

1. Sakane, A., Hamamoto, Y. and Sumimoto, T., "Behavior of Diesel Spray Impinging on a Wall," Trans. Jpn. Soc. Mech. Eng. (Series B), 54-503, pp. 1861-1865, 1978.
2. Fujimoto, H., Saito, M., Minoura, A. and Senda, J., "Characteristics of a Diesel Spray Impinging on a Flat Wall," Trans. Jpn. Soc. Mech. Eng. (Series B), 54-504, pp.2252-2259, 1978.
3. Kuniyosi, H., Yamamoto, H., Fujimoto, H. and Sato, G. T., " Investigation on the Characteristics of Diesel Fuel Spray (Third Paper : Impinging upon a Flat Plate)," Jour. of the M.E.S.J., 15-11, pp. 57-64, 1980.
4. Kawamura, K. and Saito, A., " Measurement of Particle Density Distribution in Sprays by Laser Light Computed Tomography," Tran. of the Society of Automotive Engineers of Japan, No.27, pp. 48-54, 1983.
5. Nakayama, M. and Araki, T., "Visualization of Spray Structure by Means of Computed Tomography," Proc. of COMODIA 85, pp. 131-139, 1985.
6. Nishida, K., Hiroyasu, H. and Suzuki M., "Analysis of Fuel Jet and Vaporizing Spray by Combined Schlieren and Computed Tomographic Technique," Proc. of the First KSME-JSME Thermal and Fluids Engineering Conference, Vol.1, pp. 1-

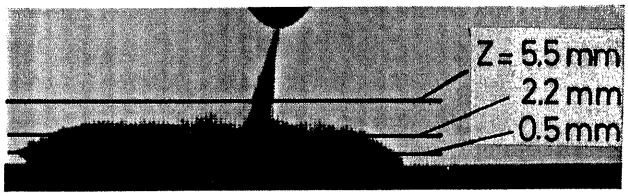

Fig.11 Shadow photograph of an impinging spray
θ=15 deg., L=13.4 mm, d_0=0.25 mm, t=1.1 ms

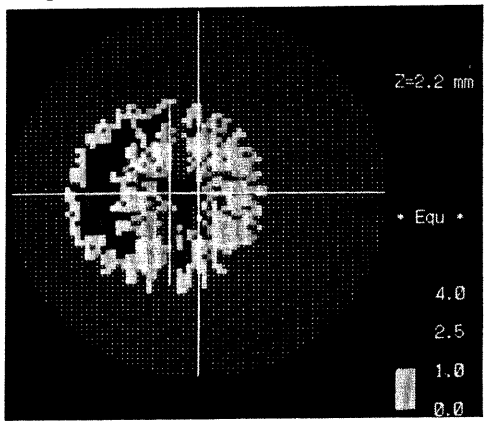

(1) Contour map of equivalence ratio
in a section parallel to the wall at Z=2.2 mm

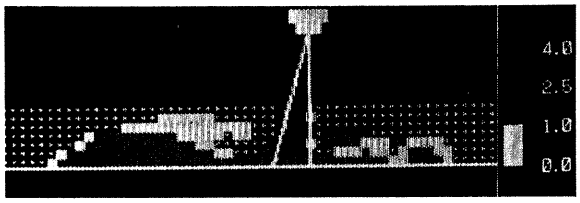

(2) Contour map of equivalence ratio
in a section normal to the wall

Fig.12 Reconstructed tomograms of
an impinging spray shown in Fig.11

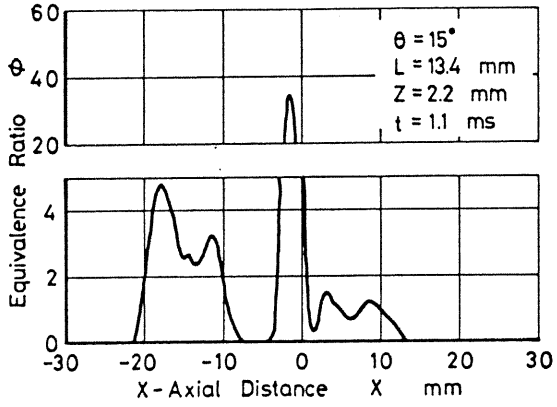

Fig.13 Distribution of equivalence ratio
along X-axis at Z=2.2 mm

423-428, 1988.

7. Ramachandran, G. N. and Lakshminarayanan, A. V., "Three-Dimensional Reconstruction from Radiographs and Electron Micrographs:Application of Convolutions instead of Fourier Transforms," Proc. Nat. Acad. Sci. USA, 68-9, pp. 2236-2240, 1971.

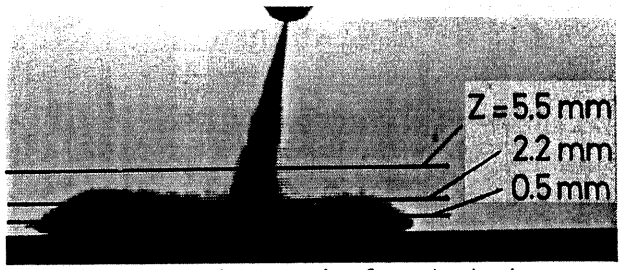

Fig.14 Shadow photograph of an impinging spray
θ=15 deg., L=20.0 mm, d_0=0.25 mm, t=1.1 ms

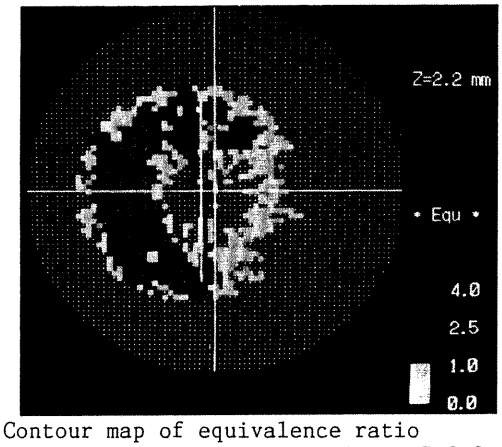

(1) Contour map of equivalence ratio
in a section parallel to the wall at Z=2.2 mm

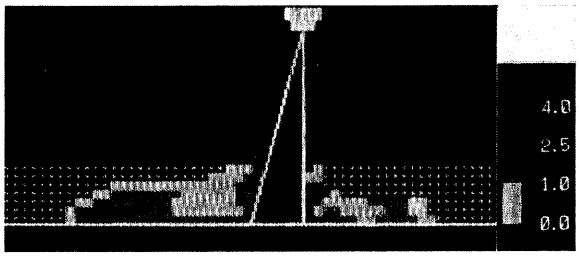

(2) Contour map of equivalence ratio
in a section normal to the wall

Fig.15 Reconstructed tomogram of
an impinging spray shown in Fig.14

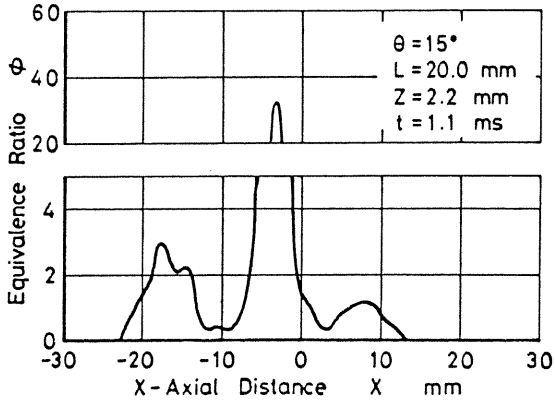

Fig.16 Distribution of equivalence ratio
along X-axis at Z=2.2 mm

8. Kamimoto, T., Ahn, S. K., Chang, Y. J., Kobayashi, H. and Matsuoka,S., "Measurement of Droplet Diameter and Fuel Concentration in a Non-Evaporating Diesel Spray by Means of an Image Analysis of Shadow Photographs," SAE Paper, No. 840276, pp. 1-9, 1984.